arXiv:0803.3265v1 [physics.plasm-ph] 22 Mar 2008

J. Plasma Physics (2008), *vol.* 00, *part* 0, *pp.* 1–17. © 2008 Cambridge University Press
DOI: 10.1017/S0963548301004989 Printed in the United Kingdom

Theory and Simulations of Whistler Wave Propagation

DASTGEER SHAIKH
Institute of Geophysics and Planetary Physics (IGPP),
University of California, Riverside, CA 92521. USA.
Email:dastgeer@ucr.edu

(Received 15 Feb 2008, Revised 25 Feb 2008)

Abstract. A linear theory of whistler wave is developed wihtin the paradigm of a two dimensional incompressible electron magnetohydrodynamics model. Exact analytic wave solutions are obtained for a small amplitude whistler wave that exhibit magnetic field topological structures consistent with the observations and our simulations in linear regime. In agreement with experiment, we find that the parallel group velocity of the wave is large compared to its perpendicular counterpart. Numerical simulations of collisional interactions demonstrate that the wave magnetic field either coalesces or repels depending upon the polarity of the associated current. In the nonlinear regime, our simulations demonstrate that the evolution of wave magnetic field is governed essentially by the nonlinear Hall force.

1. Introduction

Whistler waves are widely observed in many space and laboratory plasma phenomena. For instance, they are believed to be generated in the Earth's ionospheric region by lightning discharges and proceed in the direction of Earth's dipole magnetic field [1]. They have also been recently detected in the Earth's radiation belt by the STEREO S/WAVES instrument [2]. Moreover, there are observations of Venus' ionosphere that reveal strong, circularly polarized, electromagnetic waves with frequencies near 100Hz. The waves appear as bursts of radiation lasting 0.25 to 0.5s, and have the expected properties of whistler-mode signals generated by lightning discharges in Venus' clouds [3]. These waves are also reported near the Earth's magnetopause [4] and the Cluster spacecraft encountered them during the process of magnetic reconnection in the Earth's magnetotail region [5]. Upstream of collisionless shock, whistler waves are found to play a crucial role in heating the plasma ions [6]. Their excitation and propagation are not only limited to the Earth's nearby ionosphere, but they are also found to be excited near the ionosphere of other planets such as in the radiation belts of Jupiter and Saturn [7]. Whistler waves are believed to be a promising candidate in transporting fields and currents in plasma opening switch (POS) devices [8], which operate on fast electron time scales. Similarly, these waves have been known to drive the phenomenon of magnetic field line reconnection [9] in astrophysical plasmas [10]. Whistler waves have also been investigated in several laboratory experiments [11, 12, 13, 14, 15, 16], where they have been found to exhibit a variety of interesting features such as anisotropic propagation of phase front, strong dispersion characteristics, interaction with plasma

particles etc. A few experimental features have also been confirmed by recent three dimensional simulations [17], where it has been reported that the polarity and the amplitude of the toroidal magnetic field, in agreement with the laboratory experiments, determine the propagation direction and speed of the whistlers. These are only a few examples amongst a large body of work devoted to the study of whistler waves. Despite the large amount of efforts gone into understanding the existence and propagation of whistlers, their linear dynamics is still debated, specially in the context of complex nonlinear processes. For example, the role of whistler waves in high frequency turbulence and anisotropic spectral cascades has been debated recently [18, 19, 20, 21, 22].

Motivated by these issues, we in this paper develop a fully self-consistent linear analytic theory of whistler wave propagation. The electromagnetic whistler waves in a plasma are excited essentially by means of collective electron oscillations in presence of an external or self-consistent large scale magnetic field. Their characteristics frequency thus lies between ion- and electron-gyrofrequencies i.e., $\omega_{ci} \ll \omega \ll \omega_{ce}$, where ω_{ci} and ω_{ce} are ion- and electron-gyrofrequencies respectively. In such a frequency regime, usual magnetohydrodynamic theory becomes invalid and the plasma processes need to be described by electron magnetohydrodynamics (EMHD) theory [23]. The linear properties of EMHD are mainly governed by whistler waves, which constitute fundamental oscillatory modes of this model.

In this paper, we develop a linear analytical theory and simulation to investigate the linear propagation of a whistler wave packet and demonstrate that such waves lead to an exact solution of EMHD model. For the sake of simplicity, we restrict ourselves to a two dimensional plane where variations in the wave magnetic field are confined to the x and y directions only. The analytic results of our theory show a qualitative/quantitative agreement with the experimental observations and simulations. Such a comparison further enables us explain several experimentally observed features of the propagating whistler wave packets. We also carry out an investigation of collision of two propagating whistler wave packets to explore their mutual interaction in the context of ionospheric processes. The remainder of this paper is organized as follows. In Sec 2, governing equations of whistler waves and dispersive properties are described. In Sec 3, we describe the evolution of wave amplitude based on Fourier analytic method and numerical simulations. Section 4 describes the propagation studies of whistlers that show a remarkable agreement with the simulation in the linear regime. The linear simulations are discussed in Sec 5. Section 6 contains results of mutual interaction of two whistler modes, whereas Sec 7 describes nonlinear evolution of the whistlers. Finally conclusions are discussed in Sec 8.

2. Dynamical Equations of Whistler Waves

Whistler wave dynamics is governed essentially by the equations of EMHD. The EMHD phenomena occur typically on rapid electron time scales [23], while ions do not participate in the dynamics. Thus, the basic frequency scales involved are $\omega_{ci} \ll \omega \ll \omega_{ce}$ (where ω_{ci}, ω_{ce} are respectively ions and electrons gyro-frequencies, and ω is the characteristic frequency) and the length scales are $c/\omega_{pi} < \ell < c/\omega_{pe}$, where ω_{pi}, ω_{pe} are the plasma ion and electron frequencies. Currents carried by the electron fluid are important. Since stationary ions merely provide a neutralizing background to a quasi-neutral EMHD plasma, their momentum can be ignored in

the high frequency regime. The momentum equation of electron is

$$m_e n\left(\frac{\partial \mathbf{V}_e}{\partial t}+\mathbf{V}_e\cdot\nabla\mathbf{V}_e\right)=-en\mathbf{E}-\frac{ne}{c}\mathbf{V}_e\times\mathbf{B}-\nabla P-\mu m_e n\mathbf{V}_e, \tag{2.1}$$

$$\mathbf{E}=-\nabla\phi-\frac{1}{c}\frac{\partial\mathbf{A}}{\partial t}, \tag{2.2}$$

$$\nabla\times\mathbf{B}=\frac{4\pi}{c}\mathbf{J}+\frac{1}{c}\frac{\partial\mathbf{E}}{\partial t}, \tag{2.3}$$

$$\frac{\partial n}{\partial t}+\nabla\cdot(n\mathbf{V}_e)=0. \tag{2.4}$$

The remaining equations are $\mathbf{B}=\nabla\times\mathbf{A}, \mathbf{J}=-en\mathbf{V}_e, \nabla\cdot\mathbf{B}=0$. Here $m_e, n, \mathbf{V}_e$ are the electron mass, density and fluid velocity respectively. $\mathbf{E}, \mathbf{B}$ respectively represent electric and magnetic fields and $\phi, \mathbf{A}$ are electrostatic and electromagnetic potentials. The remaining variables and constants are, the pressure P, the collisional dissipation μ, the current due to electrons flow $\mathbf{J}$, and the velocity of light c. The displacement current in Ampere's law Eq. (2.3) is ignored, and the density is considered as constant throughout the analysis. The electron continuity equation can therefore be represented by a divergence-less electron fluid velocity $\nabla\cdot\mathbf{V}_e=0$. The electron fluid velocity can then be associated with the rotational magnetic field through

$$\mathbf{V}_e=-\frac{c}{4\pi ne}\nabla\times\mathbf{B}.$$

On taking the curl of Eq. (2.1) and, after slight rearrangement of the terms, we obtain a generalized electron momentum equation in the following form.

$$\frac{\partial\mathbf{P}}{\partial t}-\mathbf{V}_e\times(\nabla\times\mathbf{P})+\nabla\xi=-\mu m_e\mathbf{V}_e \tag{2.5}$$

where

$$\mathbf{P}=m_e\mathbf{V}_e-\frac{e\mathbf{A}}{c}\qquad\text{and}\quad\xi=\frac{1}{2}m_e\mathbf{V}_e\cdot\mathbf{V}_e+\frac{P}{n}-e\phi.$$

The curl of Eq. (2.5) leads to a three-dimensional equation of EMHD describing the evolution of the whistler wave magnetic field,

$$\frac{\partial}{\partial t}(\mathbf{B}-d_e^2\nabla^2\mathbf{B})+\mathbf{V}_e\cdot\nabla(\mathbf{B}-d_e^2\nabla^2\mathbf{B})-(\mathbf{B}-d_e^2\nabla^2\mathbf{B})\cdot\nabla\mathbf{V}_e=\mu d_e^2\nabla^2\mathbf{B}. \tag{2.6}$$

where $d_e=c/\omega_{pe}$, electron skin depth, is an intrinsic length-scale in EMHD. The three-dimensional equations of EMHD can be transformed into two dimensions by regarding variation in the $\hat{z}$-direction as ignorable i.e. $\partial/\partial z=0$, and separating the total magnetic field $\mathbf{B}$ into two scalar variables, such that $\mathbf{B}=\hat{z}\times\nabla\psi+b\hat{z}$. Here ψ and b respectively present perpendicular and parallel components of the wave magnetic field. The corresponding equations of these components can be written in a normalized form as follows,

$$\frac{\partial}{\partial t}(\psi-d_e^2\nabla^2\psi)+\hat{z}\times\nabla b\cdot\nabla(\psi-d_e^2\nabla^2\psi)-B_0\frac{\partial}{\partial y}b=0, \tag{2.7}$$

$$\frac{\partial}{\partial t}(b-d_e^2\nabla^2 b)-d_e^2\hat{z}\times\nabla b\cdot\nabla\nabla^2 b+\hat{z}\times\nabla\psi\cdot\nabla\nabla^2\psi+B_0\frac{\partial}{\partial y}\nabla^2\psi=0. \tag{2.8}$$

The length and time scales are normalized respectively by d_e and ω_{ce}, whereas magnetic field is normalized by a typical mean B_0. The linearization of Eqs. (2.7)

& (2.8) about a constant magnetic field B_0 yields the dispersion relation for the whistlers, the normal mode of oscillation in the EMHD frequency regime, and is given by

$$\omega_k = \omega_{c_0} \frac{d_e^2 k_y k}{1 + d_e^2 k^2},$$

where $\omega_{c_0} = eB_0/mc$ and $k^2 = k_x^2 + k_y^2$. From the set of the EMHD Eqs. (2.7) & (2.8), there exists an intrinsic length scale d_e, the electron inertial skin depth, which divides the entire spectrum into two regions; namely short scale ($kd_e > 1$) and long scale ($kd_e < 1$) regimes. In the regime $kd_e < 1$, the linear frequency of whistlers is $\omega_k \sim k_y k$ and the waves are dispersive. Conversely, dispersion is weak in the other regime $kd_e > 1$ since $\omega_k \sim k_y/k$ and hence the whistler wave packets interact more like the eddies of hydrodynamical fluids.

3. Evolution of Whistler Wave Amplitude

The evolution of the amplitude associated with a linear whistler wave can be studied from Eqs. (2.7) & (2.8) after dropping the nonlinear terms, as described in the following.

$$\frac{\partial}{\partial t}(\psi - \nabla^2\psi) - B_0 \frac{\partial b}{\partial y} = \mu \nabla^2 \psi \tag{3.1}$$

$$\frac{\partial}{\partial t}(b - \nabla^2 b) + B_0 \frac{\partial}{\partial y} \nabla^2 \psi = \mu \nabla^2 b. \tag{3.2}$$

The rhs of the above equations now contains a damping term. We adopt following definition to Fourier transform the evolution variables of Eqs. (3.1) & (3.2),

$$G(x, y, t) = \frac{1}{2\pi} \int_{-\infty}^{+\infty} \int_{-\infty}^{+\infty} G(k_x, k_y, t) \exp(ik_x x + ik_y y) dk_x dk_y \tag{3.3}$$

and the corresponding inverse Fourier transform is

$$G(k_x, k_y, t) = \frac{1}{2\pi} \int_{-\infty}^{+\infty} \int_{-\infty}^{+\infty} G(x, y, t) \exp(-ik_x x - ik_y y) dx dy. \tag{3.4}$$

We then write Eqs. (3.1) & (3.2) as,

$$\frac{\partial}{\partial t} \begin{pmatrix} b_k \\ \\ \psi_k \end{pmatrix} = \begin{pmatrix} \frac{-\mu k^2}{1+k^2} & \frac{ik_y B_0 k^2}{1+k^2} \\ \\ \frac{ik_y B_0}{1+k^2} & \frac{-\mu k^2}{1+k^2} \end{pmatrix} \begin{pmatrix} b_k \\ \\ \psi_k \end{pmatrix} \tag{3.5}$$

where $b_k \sim b(k_x, k_y, t)$ and $\psi_k \sim \psi(k_x, k_y, t)$. The solutions of Eq. (3.5) can be written as;

$$b_k(t) = \frac{1}{2}\left[b_k(0) + k\psi_k(0)\right] \exp(\lambda_+ t) + \frac{1}{2}\left[b_k(0) - k\psi_k(0)\right] \exp(\lambda_- t) \tag{3.6}$$

$$\psi_k(t) = \frac{1}{2k}\left[b_k(0) + k\psi_k(0)\right] \exp(\lambda_+ t) - \frac{1}{2k}\left[b_k(0) - k\psi_k(0)\right] \exp(\lambda_- t) \tag{3.7}$$

where $b_k(0)$ and $\psi_k(0)$ denote the Fourier transformed initial conditions of the variables $b(x, y, t = 0)$ and $\psi(x, y, t = 0)$ respectively, and λ is an eigen value of the

squared matrix of Eq. (3.5) which is given as below;

$$\lambda_{\pm} = \frac{-\mu k^2}{1+k^2} \pm \frac{ik_y k B_0}{1+k^2}. \tag{3.8}$$

Here also, $\pm$ sign corresponds to the wave moving in the forward and backward direction. To seek an analytic solution of Eqs. (3.6) & (3.7), we initialize the wave magnetic field perturbations by means of a current carrying antenna similar to that of Stenzil's et al [15] experiment such that there exists only in plane component of the wave magnetic field, whereas the component along the ambient magnetic field is zero initially. Accordingly, we choose the following kind of initial perturbation to study the behaviour of wave amplitude

$$\psi(x, y, t=0) = \Psi_0 \cos(ax) \exp\left(-\frac{y^2}{\sigma_y^2}\right)$$
$$b(x, y, t=0) = 0$$

Fourier transformation yields,

$$\psi_k(0) = \frac{\Psi_0 \sigma_y}{2}\sqrt{\pi}[\delta(k_x + a) + \delta(k_x - a)] \exp\left(-\frac{\sigma_y^2 k_y^2}{4}\right) \tag{3.9}$$
$$b_k(0) = 0$$

We would like to concentrate on the case in which a wave packet is propagating in the forward direction only, and hence choose the eigen value that corresponds to λ_+ in the Eq. (3.8). Under such conditions, the poloidal component of wave magnetic field i.e., Eq. (3.7) assumes the form as;

$$\psi_k(t) = \frac{1}{2}\psi_k(0) \exp(\lambda_+ t)$$

substituting Eq. (3.9) into above eqn and then inverse Fourier transformation gives

$$\psi(x, y, t) = \frac{\Psi_0 \sigma_y \sqrt{\pi}}{8\pi} \int_{-\infty}^{+\infty} [\delta(k_x + a) + \delta(k_x - a)] \exp(ik_x x)\zeta(k_x) dk_x \tag{3.10}$$

where,

$$\zeta(k_x) = \int_{-\infty}^{+\infty} \exp\left(-\frac{\sigma_y^2 k_y^2}{4}\right) \exp\left(iB_0 k k_y t\right) \exp(ik_y y) dk_y, \tag{3.11}$$

The expression of ψ contains another integral given by Eq. (3.11). We therefore first solve Eq. (3.11) and substitute the solution into Eq. (3.10). In order to do so, we put Eq. (3.11) into the following form

$$\zeta(k_x) = \int_{-\infty}^{+\infty} F(k) \exp\left[i\chi(k)t\right] dk_y \tag{3.12}$$

where $k^2 = (k_x^2 + k_y^2)$ and

$$F(k) = \exp\left(-\frac{\sigma_y^2 k_y^2}{4}\right)$$

$$\chi(k) = \omega(k) + k_y \frac{y}{t}$$

$$\omega(k) = B_0 k_y k$$

We employ the method of stationary phases [24, 25] to analyze Eq. (3.12). This method indicates that in the time asymptotic limit (i.e., at large times), the dominant contribution in the integral will essentially come from the maximum of the exponential part. This further suggests that the function $\chi(k)$ in Eq. (3.12), must take on a real and positive maximum value. Away from this maximum, the integrand will have negligibly small contribution. The condition of maximization of $\chi(k)$ further implies that

$$\frac{\partial}{\partial k_y}\chi(k) = 0. \tag{3.13}$$

The vanishing of first derivative reveals that we do have stationary points, which may be either maximum or minimum. Equation (3.13) gives a bi-quadratic algebraic equation in k_y, whose roots are basically functions of k_x.

$$k_y(k_x) = \pm\left\{\frac{y^2}{8B_0^2t^2} - \frac{k_x^2}{2} \pm \frac{y}{2B_0t}\sqrt{\frac{y^2}{16B_0^2t^2} + \frac{k_x^2}{2}}\right\}^{1/2}$$

The above equation admits four roots. We thus have four stationary points corresponding to these four roots. We take into account only that point, which gives a maximum contribution in the Eq. (3.12). We denote this point as $k_0 = k_y^{\max}(k_x)$. Taylor expanding the function $\chi(k)$ around this stationary point (k_0), we may write

$$\chi(k) = \chi(k_0) + \underbrace{(k_y - k_0)\chi'(k_0)}_{0} + \frac{1}{2!}(k_y - k_0)^2\chi''(k_0).$$

Note the second term in the expansion is zero because of the condition of extremum imposed by Eq. (3.13). Substituting $\chi(k)$ in Eq. (3.12), we get

$$\zeta(k_x) = F(k_0)\exp\left[i\chi(k_0)t\right]\int_{-\infty}^{+\infty}\exp\left[i\frac{1}{2!}(k_y - k_0)^2\chi''(k_0)t\right]dk_y.$$

Equation (3.10) with the help of above expression give,

$$\psi(x,y,t) = \frac{\Psi_0\sigma_y\sqrt{\pi}}{8\pi}\int_{-\infty}^{+\infty}\left[\delta(k_x + a) + \delta(k_x - a)\right]\exp(ik_x x) \times F(k_0)\exp\left[i\chi(k_0)t\right]\sqrt{\frac{2\pi}{t\chi''(k_0)}}dk_x \tag{3.14}$$

where we have used $\int_{-\infty}^{+\infty}\exp\left[i\frac{1}{2!}(k_y - k_0)^2\chi''(k_0)t\right]dk_y = \sqrt{\frac{2\pi}{t\chi''(k_0)}}$. The solution can be written as

$$\psi(x,y,t) = \frac{\Psi_0\sigma_y\sqrt{\pi}}{4\pi}\cos(ax)F(k_0)\exp\left[i\chi(k_0)t\right]\sqrt{\frac{2\pi}{t\chi''(k_0)}} \tag{3.15}$$

Equation (3.15) can be used to predict the behaviour of wave amplitude at a given location in space. The various quantities in this equation are as follows;

$$k_0 = \left\{\frac{y^2}{8B_0^2t^2} + \frac{y}{2B_0t}\sqrt{\frac{y^2}{16B_0^2t^2} + \frac{a^2}{2}} - \frac{a^2}{2}\right\}^{1/2}$$

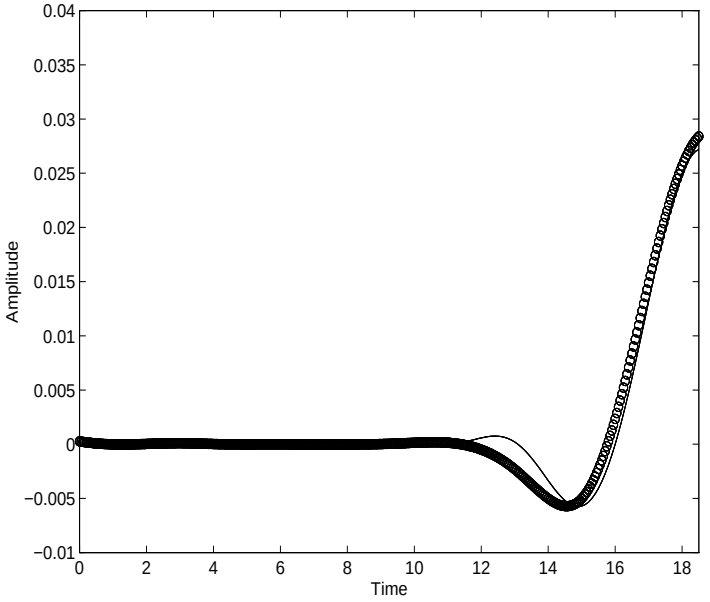

Figure 1. The behaviour of linear wave amplitude. Circle shows analytical prediction of wave amplitude, which overlaps on the amplitude obtained from numerical simulation of Eqs. (2.7) & (2.8) in the linear regime. Clearly, the analytic amplitude and that obtained from numerical simulation show an excellent agreement in a long time evolution.

$$F(k_0) = \exp\left(-\frac{\sigma_y^2 k_0^2}{4}\right)$$

$$\chi(k_0) = B_0 k_0 (k_0^2 + a^2)^{1/2} + k_0 \frac{y}{t}$$

$$\chi''(k_0) = B_0 \left[\frac{3k_0}{\sqrt{k_0^2 + a^2}} - \frac{k_0^3}{(k_0^2 + a^2)^{3/2}}\right]$$

We next numerically integrate Eqs. (2.7) & (2.8) with the help of pseudospectral code to determine the amplitude of the propagating whistler wave in the linear regime. This amplitude will then be compared with the one predicted by Eq. (3.15). The numerical code is based on the discrete Fourier representation in k-space in the two directions viz, x and y. The boundary conditions in the two directions are periodic in nature. The linear part of the equations is exactly integrated in Fourier space. On the other hand, the evaluation of nonlinear part is carried out in real space and then Fourier transform it to k-space. We use Fast Fourier Transform (FFT) routines to go back and forth in the real and k-space at each time integration step. The time advancement is done with the help of a second order leap-frog predictor corrector scheme. The numerical accuracy of the results is checked continuously by monitoring the energy conservation laws of EMHD equations at each time interval. We evolve 64^2 and/or 128^2 Fourier modes in the two dimensional box of size $20\pi \times 20\pi$ and measure the amplitude of wave at a spatial location determined by the computational box co-ordinates $(x = 9.5\pi, y = 9.5\pi)$.

A comparison of the amplitude obtained from linear simulation and stationary phase method is shown in Fig. (1). It can be seen from the figure that the two results

are in *quantitative* agreement with each other. Such a close agreement between analytical and numerical results thus clearly demonstrates the validity of the our simulation code in a linear regime.

4. Propagation Theory of Whistler Wave - Exact Wave Solutions

We now investigate the case of a propagating whistler wave packet, which is excited by a current-carrying linear wire antenna. Such a study is motivated primarily by the work described in [1-10] and specifically by the experimental observation of Ref. [15]. In these experiments [15], it has been observed that the linear whistler waves can be excited in EMHD plasma, when a current-carrying linear antenna is kept across an external magnetic field. The propagating wave packets assume conical shape whose parallel group velocity is more than the perpendicular one. Furthermore, the wave propagation has not been observed in their experiment, when the exciter was placed along the direction of an external magnetic field. In order to understand the propagation characteristics of whistler waves, we carry out both analytical as well as numerical calculations in the linear regime. We first study the evolution of wave pattern using analytical treatment.

The initial conditions are as follows;

$$\left.\begin{aligned} \psi(x,y,0) &= \Psi_0 \exp\left(-\tfrac{x^2+y^2}{\sigma^2}\right) \\ b(x,y,0) &= 0 \end{aligned}\right\} \tag{4.1}$$

where Ψ_0 and σ are amplitude and width of the distribution of the initial wave packet respectively. Equation (4.1) represents constant circular (ψ) contours of wave magnetic field in the plane of variation (i.e., in the xy-plane). Such perturbations in the xy-plane can arise as a result of a current-carrying wire antenna, which is kept parallel to the $\hat{z}$-direction. Hence there is no perturbed magnetic field along this direction. The initial condition for the axial component of the wave magnetic field is chosen to be zero, $b(x,y,t=0)=0$.

4.1. Analytical Treatment :

We Fourier transform Eq. (4.1) using the definition of Eq. (3.3) and substitute it in Eq. (3.7) to get,

$$\psi_k(t) = \frac{\Psi_0\sigma^2}{4}\exp\left(-\frac{\sigma^2k^2}{4}\right)\{\exp(\lambda_+ t)+\exp(\lambda_- t)\}$$

We inverse Fourier transform this equation and solve in the limit of $kd_e \ll 1$ and $\mu = 0$. Under these limits, the eigen values are $\lambda_\pm = \pm iB_0k_yk$, and the above eqn becomes $\psi(x,y,t) = I_+ + I_-$, where

$$I_\pm = \frac{\Psi_0\sigma^2}{8\pi}\int_{-\infty}^{+\infty}\int_{-\infty}^{+\infty} dk_x dk_y \exp(ik_x x + ik_y y)\exp\left(-\frac{\sigma^2k^2}{4}\right)\exp(\pm iB_0k_ykt)$$

We first solve I_+. Using the transformations $k_x = k\cos\theta$ and $k_y = k\sin\theta$, which give $dk_xdk_y = k\ dk\ d\theta$. The angle θ varies from 0 to 2π, while k varies from 0 to ∞. The integral I_+ then takes the form,

$$I_+ = \frac{\Psi_0\sigma^2}{8\pi}\int_0^{+\infty}\int_0^{2\pi} kdkd\theta\ \exp\left(-\frac{\sigma^2k^2}{4}\right)\exp\left[i(ky+B_0k^2t)\sin\theta\right]$$

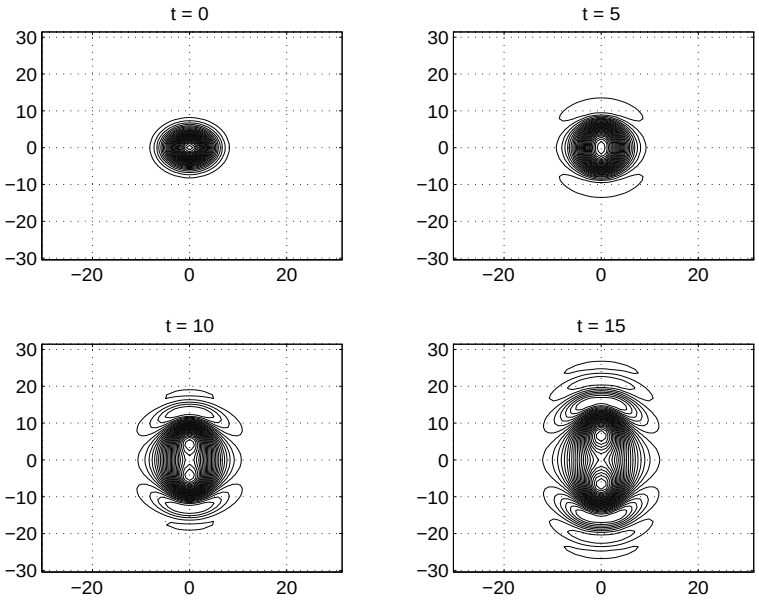

Figure 2. Propagation of whistler waves. The wave fronts have conical shape. Figure shows constant ψ-contours at various time. The vertical axis represents y-axis, along which B_0 is oriented. Horizontal axis indicates x-axis. Similar wave field topology has been reported in Ref [15].

$$\times \exp\left(ikx\cos\theta\right)$$

The exponential term containing sine in the above expression can be expanded using Bessel identity 26, $\exp(i\xi\sin\theta) = \sum_{n=-\infty}^{+\infty} J_n(\xi)\exp(in\theta)$. We thus get

$$I_+ = \frac{\Psi_0\sigma^2}{8\pi}\int_0^{+\infty}\int_0^{2\pi} kdkd\theta\exp\left(-\frac{\sigma^2k^2}{4}\right)\sum_{n=-\infty}^{+\infty} J_n(ky+B_0k^2t) \times \exp\left[i(n\theta+kx\cos\theta)\right]$$

We then carry out the θ-integral with the help of the identity [26], $\frac{i^{-n}}{2\pi}\int_0^{2\pi}\exp[i(n\theta+\beta\cos\theta)]d\theta = J_n(\beta)$, and get the equation,

$$I_+ = \frac{\Psi_0\sigma^2}{4}\int_0^{+\infty} kdk\exp\left(-\frac{\sigma^2k^2}{4}\right)\sum_{n=-\infty}^{+\infty} J_n(ky+B_0k^2t)\exp\left(\frac{in\pi}{2}\right)J_n(kx)$$

Using one of the Bessel identities [26], we then evaluate the summation of above equation. This gives us

$$I_+ = \frac{\Psi_0\sigma^2}{4}\int_0^{+\infty} kdk\exp\left(-\frac{\sigma^2k^2}{4}\right)J_0\left(\sqrt{(xk)^2+(yk+B_0k^2t)^2}\right)$$

We carry out the similar analysis to integrate I_- and get the total ψ as follows,

$$\psi(x,y,t) = \frac{\Psi_0\sigma^2}{4}\int_0^{+\infty} kdk\exp\left(-\frac{\sigma^2k^2}{4}\right)\left[J_0(\Pi_+)+J_0(\Pi_-)\right] \qquad (4.2)$$

Similarly, we solve for Eq. (3.6) and get the expression for the axial component as

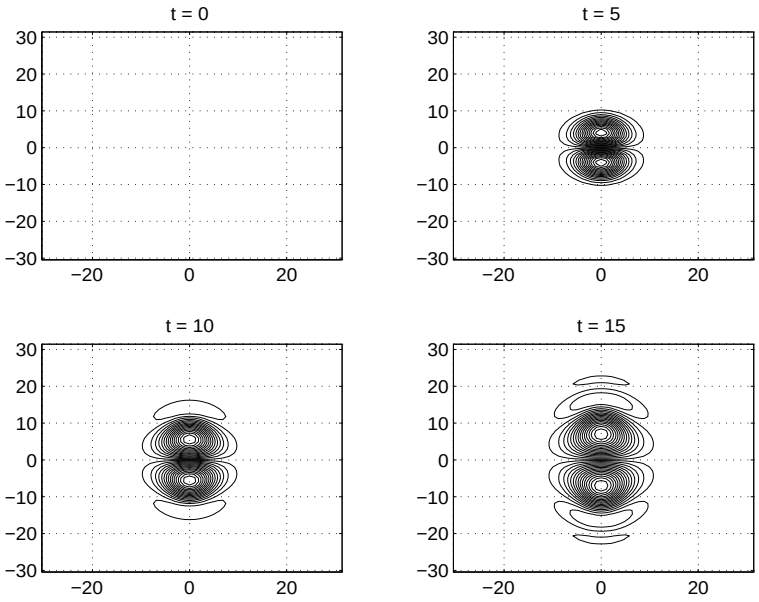

Figure 3. Constant b-contours of magnetic field of propagating whistler waves. Note that the b component is zero initially, and is generated later by means of linear mode coupling process.

follows,

$$b(x,y,t) = \frac{\Psi_0\sigma^2}{4}\int_0^{+\infty} dk \exp\left(-\frac{\sigma^2k^2}{4}\right)\left[J_0(\Pi_+) - J_0(\Pi_-)\right] \tag{4.3}$$

where $\Pi_\pm = \sqrt{(xk)^2 + (yk \pm B_0k^2t)^2}$. Equations (4.2) & (4.3) form an exact whistler wave solution of the EMHD model representing respectively the evolution of poloidal and axial components of wave magnetic field. The substitution of $t = 0$ in Eqs. (4.2) & (4.3) retrieves the initial condition i.e., Eq. (4.1). The numerical integration of Eqs. (4.2) & (4.3) at various time are displayed in Figs. (2) & (3). It is clear from the figures that the propagating wave fronts are conical in shape. It can be noticed from Fig. (3) that the axial component, though absent initially (i.e., at $t = 0$), acquires a finite amplitude during propagation.

The axial component of wave field is generated primarily due to linear coupling in the equations representing the evolution of b and ψ (i.e., Eqs. (3.2) & (3.1)). The topology of the magnetic field in the propagating wave packet is consistent with Ref [15].

5. Simulation of Linear Wave Propagation

We now carry out numerical simulation of low amplitude whistler waves. The initial condition is the same as that used earlier in the analytical treatment. However, unlike the linearized approximation (Eqs. (3.2) & (3.1)) used earlier to obtain the analytical expression for the evolved fields, here we make use of the exact Eqs. (2.7) & (2.8) for simulation. At small amplitude we expect the linear approximation to be valid, and hence an agreement of the simulation results with those presented in the earlier section.

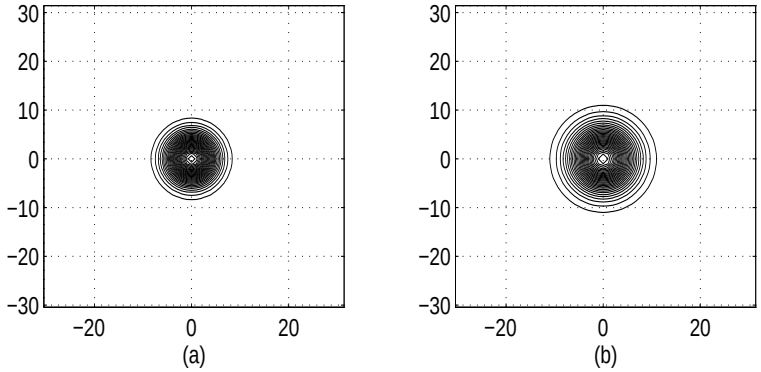

Figure 4. Diffusion of wave magnetic field, when the exciter is parallel to B_0. (a) represents constant contours of perturbed magnetic field at $t = 0$ and (b) shows the diffusion of initial field at $t = 20$ unit of time.

In the absence of B_0, the fields simply diffuse as shown in Fig. (4). This configuration can be viewed as identical to that of the Ref [15] wherein the linear wire antenna is kept parallel to the external magnetic field. The field lines merely diffuse in such a scenario. The other case of linear wire antenna being placed across an external magnetic field can be simulated by choosing B_0 as finite. In this case we observe propagating whistler wave packets with asymmetric orientation in the xy-plane. The phase fronts have conical shape as reported both in our approximate linear analytical treatment of the problem as also in experiments. This can be understood by realising that the fronts move faster along $\hat{y}$ (direction of external magnetic field) than across. This also shows clearly that the group velocity along B_0 is larger than the perpendicular group velocity. A quantitative estimation of

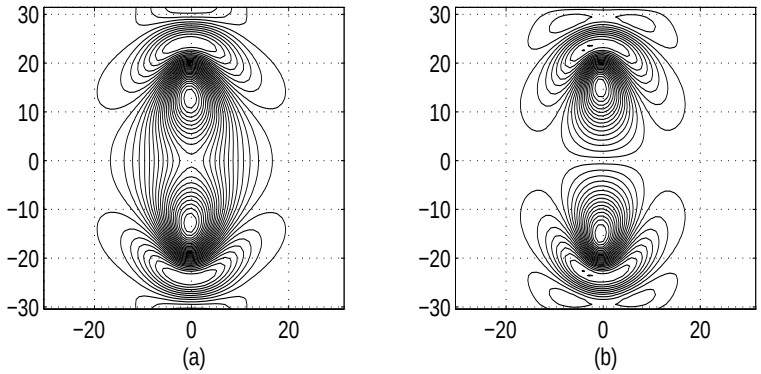

Figure 5. Propagation of whistler waves recorded at time $t = 20$. (a) ψ-field, (b) b-field contours.

the group velocities of the propagating whistler wave packet in the two directions i.e., parallel and perpendicular to B_0 can be carried out as follows. The two group velocities can be computed from the dispersion relation. The perpendicular group velocity ($V_{G_\perp}$) can be given as

$$V_{G_\perp} = \frac{\partial \omega}{\partial k_x} = \frac{B_0 k_y k_x}{k(1+k^2)} - \frac{2k k_x k_y B_0}{(1+k^2)^2}. \tag{5.1}$$

The typical wave numbers k_x and k_y in the above equation can be estimated as σ_x^{-1} and σ_y^{-1} respectively, which represent the width of initial Gaussian distribution of the wave packet. Replacing k_x and k_y by σ_x^{-1} and σ_y^{-1} respectively in Eq. (5.1), we get

$$V_{G_\perp} = \frac{B_0/\sigma_x\sigma_y}{\sqrt{\frac{1}{\sigma_x^2}+\frac{1}{\sigma_y^2}}\left\{1+\left(\frac{1}{\sigma_x^2}+\frac{1}{\sigma_y^2}\right)\right\}} - \frac{\frac{2B_0}{\sigma_x\sigma_y}\sqrt{\frac{1}{\sigma_x^2}+\frac{1}{\sigma_y^2}}}{\left\{1+\left(\frac{1}{\sigma_x^2}+\frac{1}{\sigma_y^2}\right)\right\}^2} \tag{5.2}$$

Similarly, the parallel group velocity gives,

$$V_{G_\parallel} = \frac{B_0}{\sqrt{\frac{1}{\sigma_x^2}+\frac{1}{\sigma_y^2}}\left(1+\frac{1}{\sigma_x^2}+\frac{1}{\sigma_y^2}\right)^2}\left\{\left(1-\frac{1}{\sigma_x^2}-\frac{1}{\sigma_y^2}\right)\frac{1}{\sigma_y^2}+\left(1+\frac{1}{\sigma_x^2}+\frac{1}{\sigma_y^2}\right)\left(\frac{1}{\sigma_x^2}+\frac{1}{\sigma_y^2}\right)\right\} \tag{5.3}$$

We had chosen in the simulation, $\sigma_x^2 = \sigma_y^2 = 20.0$ and $B_0 = 1.0$, which yields $V_{G_\perp} = 0.14$ and $V_{G_\parallel} = 0.41$, thereby clearly indicating that $V_{G_\parallel} > V_{G_\perp}$. It is because of the larger parallel group speed, the wave magnetic field structures are conical and they propagate along the direction of the ambient magnetic field.

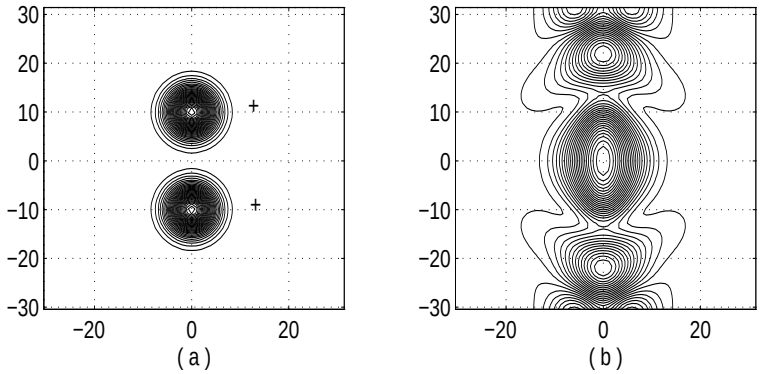

Figure 6. Interaction of two whistler wave packets excited by parallel currents in the two antennae show an attraction. Figure (a) shows the wave fields at $t = 0$ and figure (b) represent the field at $t = 20$.

6. Collisional Interaction of Two Whistlers

We now study the collisional interaction between whistler wave packets. Such interactions can possibly exist in the Earth's ionosphere where the oppositely traveling waves along the Earth's dipole magnetic field collide. In a laboratory plasma, such an interaction can be studied by exciting the wave field from the two linear wire antennae separated by a finite distance. The currents carried by the oppositely traveling waves are either parallel or anti-parallel to each other. Our objective here is to investigate as what kind of resultant state would be borne out from such interactions. When initial excitation is due to the antennae current flowing in the same direction (i.e., parallel currents in the antennae), they give rise to wave fields of similar signs in the plasma. This is shown in Fig. (6)(a). The evolution of the

two wave packets then leads to the formation of a magnetic null line. The magnetic pressure being weak at the central region, there is a tendency of attraction between the magnetic configuration caused by the two currents. Along with this attraction as the whistler waves get excited and propagate, the null line at the center alters and forms an *O*-point (see Fig. (6)(b)). The attraction of wave magnetic fields can also be understood as follows. The wave magnetic field induces parallel currents in the plasma, which then attract each other. This can be contrasted with Fig. (7) where the initial excitation are due to the anti-parallel currents in the two wire antennae. It is observed that there is no such magnetic null line for this case, albeit here the magnetic field maximizes in the centeral region, causing repulsion. It can be clearly seen that in this case there is no formation of *O*-point at the center. This is shown in Fig. (7)(a,b). In this case, the wave fields induces anti-parallel currents, which repel each other.

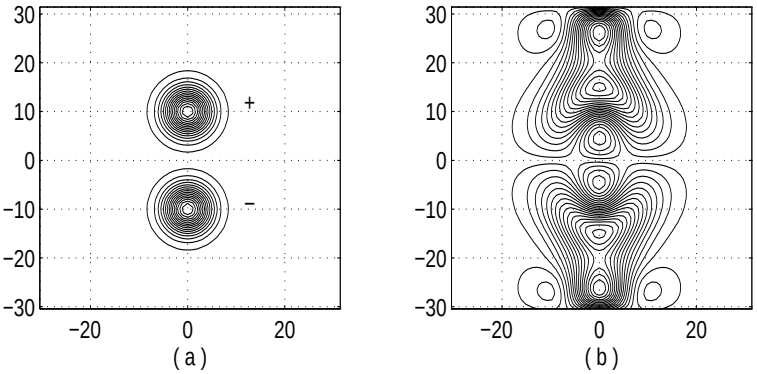

Figure 7. Two whistler wave packets launched by anti-parallel currents in the two wire antennae repel each other. Figures (a,b) show the wave fields respectively at $t = 0$ and $t = 20$.

7. Nonlinear Whistler Waves

In the previous section we have presented detailed studies on the propagation and collision of whistler waves, when the amplitude of initial perturbation was smaller than the external magnetic field (B_0). We now carry out our investigation, when the amplitude of the perturbed field is comparable or greater than the ambient magnetic field (B_0). This is the regime where nonlinear interactions may be of great importance. Nonlinear excitation of whistler in laboratory plasmas has n't been yet understood fully [16]. We therefore undertake this study to understand nonlinear evolution of whistlers. Our choice of initial field perturbation is identical to the one discussed in the previous sections, which was also consistent with the excitation mechanism adopted in the experiments [15, 16]. In this section we choose to study the evolution of the similar initial perturbation, however, now the perturbed field has an amplitude which is comparable or larger than the ambient field B_0. Figure (8) shows the initial and the evolved field configurations. Clearly the magnetic field topology is distorted and distinct from the linear results presented earlier (see Fig. (2), Fig. (5)(a)).

The distortion (or modification) in the propagation characteristics of whistler

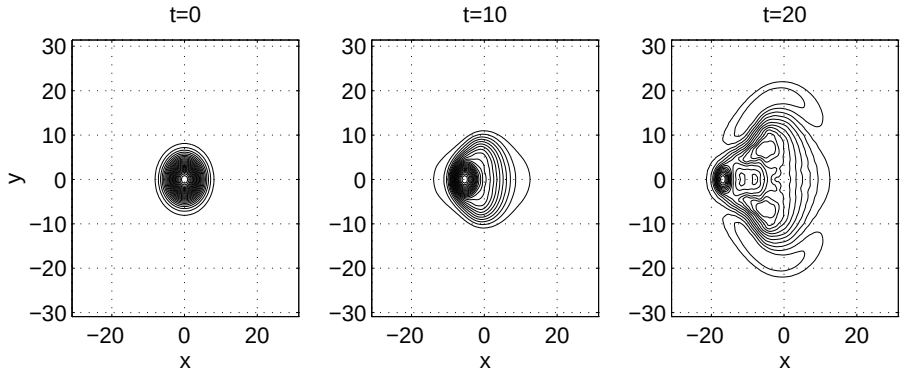

Figure 8. Large amplitude whistler wave. The wave field is distorted in $-x$ direction due to experiencing a net $\mathbf{J} \times \mathbf{B}$ force.

waves can be understood as follows. The linear wire antenna, which induces the wave magnetic field in the xy-plane of variation, essentially carries current ($\mathbf{J}$) along positive $\hat{z}$-direction i.e., out of plane of the page. A constant magnetic field (B_0) is already present in the $\hat{y}$-direction. This ambient magnetic field interacts with the antenna current, and gives rise to a net $\mathbf{J} \times \mathbf{B}_0$ force, which is directed along $-\hat{x}$ direction. Since the nonlinearities are at work in the large amplitude simulation, they exert the resultant Lorentz force (i.e., $\mathbf{J} \times \mathbf{B}$ force) on the wave field. The induced magnetic field of the wave thereby get influenced by the Lorentz force and consequently show a tendency to move in the direction of this force. Furthermore, a combined action of the wave motion along $\hat{y}$-direction and the push in $-\hat{x}$ direction, overall results in slight distortion of the wave field topology. This is indeed what we observe in the simulation also (see Fig. (8) at $t = 20$). Our numerical investigations, thus demonstrate that nonlinear interactions significantly influence the propagation properties of whistler waves in EMHD.

Nonlinear evolution of whistler waves is widely observed in many ionospheric and magnetospheric phenomena. For instance, whisther mode has been reported in the context of equatorial region of Earth's magnetosphere based on a modulational instability analysis [27], where it was shown that amplitude modulation in whistlers develops on much faster time scale than the wave transit period. Nonlinear interaction of whistlers is also likely to occur with magnetosonic fluctuations [28]. On the other hand, the nonlinear whistlers can potentially excite electrostatic low-frequency collisional gradient drift modes that are relevant to understanding the density irregularities in the lower part of the ionosphere [29]. Additionally, electromagnetic whistler wave, propagating parallel to an external magnetic field, are also reported to decay into another circularly polarized electromagnetic wave and an ion acoustic wave in a homogeneous plasma [30]. This result remains unaltered under the combined effects of the relativistic-mass and ponderomotive-force nonlinearities [31]. Whistler waves in inhomogeneous media play a critical role in ionospheric density striations [32]. Our simulations of nonlinear evolution of whistler waves, relevant to understanding a number of features described in the above work, thus reveal that it is the hall force corresponding to the $\mathbf{J} \times \mathbf{B}$ term in electron momentum equation that plays a crucial role and it is responsible for governing the nonlinear interactions associated with the electron whistler modes.

8. Conclusion

In conclusion, we have carried out a detailed study of whistler wave propagation with the prime objective to understand their interaction and the nonlinear propagation characteristics. For this purpose a variety of initial configuration were envisaged and their evolution studied. Whistler waves being dispersive, in the linear small amplitude limit different modes of the wave packet propagate with different phase velocities. However, the entire wave front moves with the typical group velocity. The shape of the wave front is finally governed by the group speed. The linear propagation characteristics are found to be in agreement with the experimental observations. In the nonlinear regime we show that the propagation is significantly altered. This indicates the importance as well as the subtle role of nonlinearity in the context of whistler wave propagation thereby countering earlier speculations and statements about robustness of these modes against nonlinear effects. Our studies presented in this paper can be useful in understanding a number of processes associated with the linear whistler waves, their mutual interaction and nonlinear feature in the context of interplanetary ionospheres and radiation belts.

References

[1] Helliwell, A., Whistlers and Related Ionospheric Phenomena. Standford University Press, Standford, CA. (1965).

[2] Cattell, C.; Wygant, J. R.; Goetz, K.; Kersten, K.; Kellogg, P. J.; von Rosenvinge, T.; Bale, S. D.; Roth, I.; Temerin, M.; Hudson, M. K.; Mewaldt, R. A.; Wiedenbeck, M.; Maksimovic, M.; Ergun, R.; Acuna, M.; Russell, C. T., Discovery of very large amplitude whistler-mode waves in Earth's radiation belts. *Geophys. Res. Lett.*, **35**, L01105 (2008).

[3] Russell, C. T.; Zhang, T. L.; Delva, M.; Magnes, W.; Strangeway, R. J.; Wei, H. Y., Lightning on Venus inferred from whistler-mode waves in the ionosphere. *Nature*, **450**, Issue 7170, 661-662 (2007).

[4] Stenberg, G.; Oscarsson, T.; Andr, M.; Vaivads, A.; Backrud-Ivgren, M.; Khotyaintsev, Y.; Rosenqvist, L.; Sahraoui, F.; Cornilleau-Wehrlin, N.; Fazakerley, A.; Lundin, R.; Dcrau, P. M. E., Internal structure and spatial dimensions of whistler wave regions in the magnetopause boundary layer. *Annales Geophysicae*, **25**, 11, 2439-2451 (2007).

[5] Wei, X. H.; Cao, J. B.; Zhou, G. C.; Santolk, O.; Rme, H.; Dandouras, I.; Cornilleau-Wehrlin, N.; Lucek, E.; Carr, C. M.; Fazakerley, A., Cluster observations of waves in the whistler frequency range associated with magnetic reconnection in the Earth's magnetotail. *Journal of Geophysical Research*, **112**, A10, A10225 (2007).

[6] Scholer, M., and Burgess, D., Whistler waves, core ion heating, and nonstationarity in oblique collisionless shocks. *Phys. Plasmas*, **14**, 072103-072103-11 (2007).

[7] Bespalov, P. A., Excitation of whistler waves in three spectral bands in the radiation belts of Jupiter and Saturn. *European Planetary Science Congress*, Berlin, Germany, 18 - 22 September 2006., p.461 (2006).

[8] Mason, R. J., Auer, P. L., Sudan, R. N., Oliver, B. E., Ceyler, C. E., and Greenly, J. B., Nonlinear magnetic field transport in opening switch plasmas. *Phys Fluids* B **5** 1115 (1993).

[9] Bulanov, S. V., Pegoraro, F., and Sakharov, A. S., Magnetic reconnection in electron magnetohydrodynamics. *Phys. Fluids*, B **4** 2499 (1992).

[10] Zhou, H. B., Papadopolous, K., Sharma A. S., and Chang, C. L., *Phys. Plasmas*, **3** 1484 (1996).

[11] Stenzel, R. L., Whistler wave propagation in a large magnetoplasma. *Phys. Fluids*, **19**, No. 6, 857 (1976).

[12] Stenzel, R. L., Self-ducting of large-amplitude whistler waves. *Phy. Rew. Lett.*, **35**, No. 9, 574 (1975).

[13] Urrutia J. M. and Stenzel, R. L., Transport of Current by Whistler Waves. *Phy. Rev. Lett.*, **62**, No. 3, 272 (1988).

[14] Stenzel, R. L., Urrutia, J. M., Force-free electromagnetic pulses in a laboratory plasma. *Phy. Rev. Lett.*, **65**, No. 16, 2011 (1990).

[15] Stenzel, R. L., Urrutia, J. M., and Rousculp, C. L., Pulsed currents carried by whistlers. I - Excitation by magnetic antennas. *Phys. Fluids*, B **5**, No. 2, 325 (1993).

[16] Urrutia, J. M., Stenzel, R. L., and Rousculp, C. L., Pulsed currents carried by whistlers. II. Excitation by biased electrodes. *Phys. Plasmas*, **1**, No. 5, 1432 (1994).

[17] Eliasson, B.; Shukla, P. K., Dynamics of Whistler Spheromaks in Magnetized Plasmas. *Phys. Rev. Lett.* **99**, 205005 (2007).

[18] Shaikh, D., Das, A., Kaw, P. K., Diamond, P., Whistlerization and anisotropy in two-dimensional electron magnetohydrodynamic turbulence. *Phys. Plasmas* **7**, 571 (2000).

[19] Shaikh, D., Das, A., and Kaw, P. K., Hydrodynamic regime of two-dimensional electron magnetohydrodynamics. *Phys. Plasmas* **7**, 1366 (2000).

[20] Shaikh, D., and Zank, G. P., Anisotropic Turbulence in Two-dimensional Electron Magnetohydrodynamics. *Astrophys. J.* **599**, 715 (2003).

[21] Shaikh, D., Generation of Coherent Structures in Electron Magnetohydrodynamics. *Physica Scripta*, **69**, 216 (2004).

[22] Shaikh, D., and Zank, G. P., Driven dissipative whistler wave turbulence. *Phys. Plasmas* **12**, 122310 (2005).

[23] Kingsep, A. S., Chukbar, K. V., and Yan'kov V. V. Reviews of Plasma Physics. Consultants Bureau, New York, Vol **16** (1990).
Gordeev, A. V., Kingsep, A. S., and Rudakov, L. I., *Phys. Reports*, **243**, 215–315 (1994).

[24] Arfken, G. B., and Weber, H. J., Mathematical Methods for Physicists. Academic Press Inc, USA, (1995).

[25] Witham, G. B., Linear and Nonlinear Waves, John Wiley *&* Sons, Inc, Pg. 371, (1974).

[26] Gradsteyn, I. S., and Rhyzik, I. M., Table of Integrals Series, and Products. Academic Press Inc. (1994).

[27] Shukla, P. K., Modulational instability of whistler-mode signals *Nature* **274**, 874 (1978).

[28] Stenflo, L.; Yu, M. Y.; Shukla, P. K., Electromagnetic modulations of electron whistlers in plasmas. *J. Plasma Phys.* **36**, 447 (1986).

[29] Stenflo, L.; Shukla, P. K.; Yu, M. Y., Excitation of electrostatic fluctuations by thermal modulation of whistlers. *J. Gepophys. Res.* **91**, 11369 (1986).

[30] Shukla, P. K.; Yu, M. Y.; Spatschek, K. H., Brillouin backscattering instability in magnetized plasmas. *Phys. Fluids* **18**, 265 (1975).

[31] Shukla, P. K.; Stenflo, L., Nonlinear propagation of electromagnetic waves in magnetized plasmas. *Phys. Rev. A* **30**, 2110 (1984).

[32] Shukla, P. K.; Stenflo, L., Electron magnetohydrodynamics of inhomogeneous plasmas. *Phys. Lett. A*, **259**, 49 (1999).